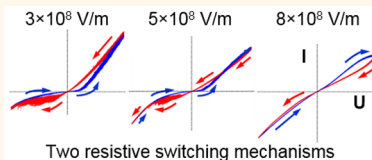


# Uncovering Two Competing Switching Mechanisms for Epitaxial and Ultrathin Strontium Titanate-Based Resistive Switching Bits

Markus Kubicek,\* Rafael Schmitt, Felix Messerschmitt, and Jennifer L. M. Rupp

Electrochemical Materials, ETH Zurich, Hönggerberg 64, 8093 Zurich, Switzerland

**ABSTRACT** Resistive switches based on anionic electronic conducting oxides are promising devices to replace transistor-based memories due to their excellent scalability and low power consumption. In this study, we create a model switching system by manufacturing resistive switches based on ultrathin 5 nm, epitaxial, and grain boundary-free strontium titanate thin films with subnanometer surface roughness. For our model devices, we unveil two competing nonvolatile resistive switching processes being of different polarities: one switching in clockwise and the other in counterclockwise direction. They can be activated selectively with respect to the effective switching voltage and time applied to the device. Combined analysis of both processes with electrical DC-methods and electrochemical impedance spectroscopy reveals that the first resistive switching process is filament-based and exhibits counterclockwise bipolar resistive switching. The  $R_{OFF}/R_{ON}$  resistance ratio of this process is extremely stable and can be tuned in the range 5–25 depending on the switching voltage and time. Excitingly, at high electric field strength a second bipolar resistive switching process was found. This process is clockwise and, therefore, reveals the opposite polarity switching direction when compared to the first one. Both processes do not obstruct each other, consequently, stable 1, 2, or even 3 crossover current–voltage ( $I$ – $V$ ) characteristics can be addressed for the memory bits. Equivalent circuit model analysis and fitting of impedance characteristics unequivocally show for the created grain boundary free switches that the oxide's defects and its carrier distribution close to the electrode interface contribute to the resistive switching mechanism. The addressability of two sets of resistive ON and OFF states in one device through electric field strength and switching time offers exciting new operation schemes for memory devices.



**KEYWORDS:** resistive switching · thin films · switching mechanism · dielectric properties · impedance spectroscopy · epitaxial growth

Oxide-based resistive switching devices have caught a lot of attention as a new class of nonvolatile resistive random access memories (ReRAM) being an alternative to classic transistor-based memories.<sup>1–4</sup> Even though first observations of oxides that can be switched in their resistive state have already been reported back in the 1960s,<sup>5,6</sup> the connection between the concept of a memristor<sup>7</sup> and resistive switches operated by charge carrier flux alterations was first presented in 2008.<sup>3</sup> In resistive switches, hysteretic current–voltage characteristics allow nonvolatile modulations between high and low resistance states at ns-switching speed.<sup>8</sup> In particular, the high scalability of simple metal|oxide|metal memristive structures and their low energy consumption surpass today's transistor-based memories.<sup>2,4,8</sup> Among the plethora of materials showing resistive

switching, mixed conducting anionic-electronic oxides rely predominantly on transport of oxygen vacancies and electronic carriers driven by high local electric field strength to modulate their resistance. The valence change of metal cations is the shared mechanistic feature of the anionic-electronic resistive switches. In accordance with that valence change, several processes are reported in literature for different material combinations in the metal|oxide|metal devices. Examples include for perovskite oxides: the redistribution of point defects,<sup>9–12</sup> creation or change of extended defects,<sup>13–17</sup> formation of conductive filaments,<sup>18–20</sup> charge-transfer resistances from interfaces such as Schottky barriers,<sup>21,22</sup> oxygen exchange with the surrounding media,<sup>9</sup> electronic trapping or tunneling effects.<sup>21,23</sup> Importantly, the resistive switching response or memristive characteristics are controlled

\* Address correspondence to markus.kubicek@mat.ethz.ch.

Received for review May 7, 2015 and accepted October 8, 2015.

Published online October 08, 2015  
10.1021/acsnano.5b02752

© 2015 American Chemical Society

by nonequilibrium transport and kinetics: The hysteretic current–voltage response depends on the flux of electrons and oxygen ions, polarity, and overall carrier concentrations. In selected material cases, also local temperature changes due to Joule heating,<sup>19,24</sup> humidity and hydratization of oxides,<sup>25,26</sup> or optical interactions<sup>27</sup> can strongly affect resistive switching characteristics and mechanisms. Besides the material choice, the film growth, crystallinity, and nonstoichiometry of the oxide play an important role on the device's transport properties, *i.e.*, introduced defects at interfaces or lattice strain lead to local compositional gradients and ionic near order modulations.<sup>28–30</sup> Even though many mechanisms were suggested, it remains often unpredictable if and how new anionic-electronic conducting metal oxides exhibit resistive switching. Uncovering the fundamentals on the charge carrier contribution, defects and diffusion kinetics form the basis to select new switching materials and provide novel flexible device operation guidelines. In literature, the focus is often laid on characterizing device operation and performance parameters such as long-term stability, resistance ON/OFF ratio, cyclability, or retention. However, the essence of a resistive switch (or memristor) being the field strength-dependent ionic carrier-flux requires attention with model experiments unveiling the switching mechanisms with respect to charge carriers, microstructures, and interfaces involved.

In the following, we carry out a systematic electrochemical study on the resistive switching mechanisms, thus analyzing their frequency and electric field strength dependencies for  $\text{SrTiO}_{3-\delta}$  bits. We design model resistive switching structures using epitaxially grown and ultrathin oxide layers of only 5 nm thickness.  $\text{SrTiO}_{3-\delta}$  was selected as a material, as it is a well-described model system for defect chemistry<sup>31–33</sup> and is also known to exhibit resistive switching.<sup>9,13,15,20,23</sup> Through the choice of epitaxial growth, with a clear microstructural definition of the oxide bulk, interfaces, and surfaces, we can treat the switching bits as oxide model case. This enables a detailed electrochemical investigation of the resistive switching mechanisms for ultrathin, oriented, and grain boundary-free  $\text{SrTiO}_{3-\delta}$  bits. Here, we employ a wide range of electrochemical methods to investigate in detail the switching processes, addressable resistive states, and capacitive contributions with respect to frequency and electric field strength. Analyses of the complex dielectric response were performed separating the materials' different resistive and capacitive contributions while connecting to the device properties such as the ON and OFF states and SET and RESET conditions. Through electrochemical investigation at low read bias and also at the off-equilibrium conditions at the switching processes, we can uniquely identify two different bipolar and nonvolatile resistive switching processes

being of different polarities: one switching clockwise and the other counterclockwise. These processes can be activated selectively with respect to the effective voltage and time scales applied to the device. In accordance, the characteristics of stable ON and OFF states addressable *via* 1, 2, or even 3 crossover current–voltage ( $I$ – $V$ ) profiles are discussed. Electrochemical circuit models describing the two different switching processes are employed in order to describe and fit the different ON and OFF states. The epitaxial and ultrathin 5 nm growth allows for a description of the polarity-dependent and defect-induced resistive switching processes of the oxide as pure crystalline bulk (excluding grain boundaries). The importance of describing the different resistive switching processes in oxygen anionic-electronic conducting  $\text{SrTiO}_{3-\delta}$  memories, highlighted in particular by results from time and electric field strength dependence of the valence changes, implicates better mechanistic understanding for optimized device operation such as low-energy switching<sup>2</sup> or multibit operation.<sup>4,34</sup>

## RESULTS AND DISCUSSION

**Device Fabrication and Characterization of Ultrathin and Epitaxial  $\text{SrTiO}_{3-\delta}$  Resistive Switching Bits.** We grow and microfabricate thin-film  $\text{SrTiO}_{3-\delta}$ -based bit structures with subnanometer surface roughness, which are grain boundary-free through epitaxial growth on a  $\text{LaNiO}_3$  thin-film bottom electrode and an underlying  $\text{LaAlO}_3$  single crystal. Figure 1a shows a schematic of the layer sequence for the oxides and electric contacting of single  $\text{SrTiO}_{3-\delta}$  memristive bits *via* the  $\text{LaNiO}_3$  bottom electrode and micropatterned Pt top electrodes.

The high-resolution transmission electron microscopy (HR-TEM) cross-section image in Figure 1b reveals the successfully grown (100) oriented and grain boundary-free epitaxial pulsed laser deposited (PLD) layers,  $\text{LaNiO}_3$  and  $\text{SrTiO}_{3-\delta}$ . The same characteristics were observed over the whole length of the focused ion beam (FIB)-cut lamella. The color contrast in the image is caused by different atomic numbers in the perovskites and allows identification of the individual layers in Figure 1b. We determine the layer thicknesses of 10 nm for the bottom electrode  $\text{LaNiO}_3$ , of 5 nm for the switching oxide  $\text{SrTiO}_3$  and of 80 nm for the Pt metal top electrode in the layer sequence of a selected  $\text{LaAlO}_3|\text{LaNiO}_3|\text{SrTiO}_{3-\delta}|\text{Pt}$  bit. To confirm the microstructural stability of the device model structures under current load, we characterized the layer stack and its material nanostructures by TEM after device operation and electrochemical characterization.

The surface of the grown  $\text{SrTiO}_{3-\delta}$  oxide was investigated by atomic force microscopy (AFM), as shown in Figure 1c. The measured surfaces are characterized by extremely low roughness of  $R_{\text{RMS}} = 0.12 \text{ nm}$  with unit cell height steps of  $\sim 0.4 \text{ nm}$ . The latter originate from

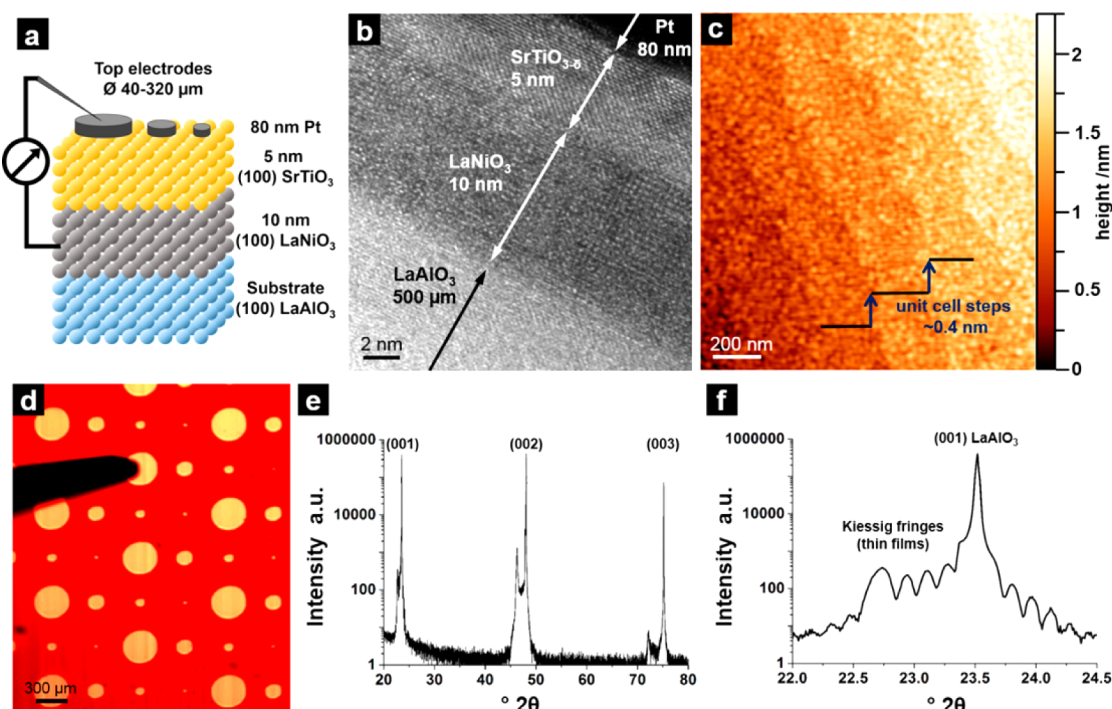


**Figure 1.** (a) Schematic of the device setup using epitaxial thin films. (b) TEM image of a cross section from underneath an electrode showing epitaxial growth of both the LaNiO<sub>3</sub> and SrTiO<sub>3-δ</sub> thin films. (c) AFM height profile of the SrTiO<sub>3-δ</sub> surface showing a flat surface with unit cell height steps. (d) Optical micrograph of the sample surface showing differently sized circular Pt-top electrodes and a Pt contacting tip. (e) X-ray diffractogram of a LaAlO<sub>3</sub>|LaNiO<sub>3</sub>|SrTiO<sub>3-δ</sub> sample before Pt-deposition showing only (00l) peaks of the highly oriented substrate and thin films. (f) Magnification of the area  $22.0^\circ < 2\theta < 24.5^\circ$  showing intensity oscillations caused by X-ray reflection (Kiessig fringes).

the small miscut angle  $<0.5^\circ$  of the (100) LaAlO<sub>3</sub> single crystal substrate. This confirms, together with the absence of islands and in accordance with HR-TEM images, epitaxial layer growth<sup>35</sup> of both, LaNiO<sub>3</sub> and SrTiO<sub>3-δ</sub>, thin films. No defects or grain boundaries were visible in the investigated areas. Hence, a nanoscopically flat and grain boundary-free array of LaNiO<sub>3</sub>|SrTiO<sub>3-δ</sub>|Pt bits was fabricated as model switches for our electrochemical investigations. In Figure 1d, we exemplify a top-view of the typical device setups for electrical measurements in an optical micrograph with differently sized Pt top microelectrodes ( $40, 80, 160, 320 \mu\text{m}$  diameter) and a Pt tip for contacting.

The X-ray diffraction (XRD) patterns of the LaNiO<sub>3</sub>/SrTiO<sub>3-δ</sub> thin-film bilayer grown on (100) LaAlO<sub>3</sub> single crystals are shown in Figure 1e,f. In the overview diffractogram (Figure 1e) only (00l)-peaks of the LaAlO<sub>3</sub>, SrTiO<sub>3</sub> and LaNiO<sub>3</sub> perovskite phases are present, showing that both thin films are grown highly oriented. A mismatch in pseudocubic lattice parameters is present in the series LaAlO<sub>3</sub>  $<^{1.6\%}$  LaNiO<sub>3</sub>  $<^{1.4\%}$  SrTiO<sub>3-δ</sub>,<sup>36–38</sup> and therefore in-plane compressive strain is expected in the SrTiO<sub>3-δ</sub> film lattice. A magnification of the diffraction pattern in Figure 1f reveals intensity oscillations around the (001) main peak of LaAlO<sub>3</sub>. These oscillations relate to constructive and destructive interference of X-ray reflections at the interfaces LaAlO<sub>3</sub>|LaNiO<sub>3</sub> and LaNiO<sub>3</sub>|SrTiO<sub>3-δ</sub>, also called Kiessig fringes.<sup>39</sup> Existence

of these fringes confirms high quality of the flat and parallel interfaces.

The fabricated LaNiO<sub>3</sub>|SrTiO<sub>3-δ</sub>|Pt bits are well-suited resistive switching model structures for electrochemical studies to gain insights on the switching mechanism and defects involved, based on the following characteristics:

- (i) Subnanometer surface roughness and precise thickness control for 5 nm SrTiO<sub>3-δ</sub> thin films allows equal switching condition over the whole electrode area.
- (ii) Epitaxial oxides with clear absence of grain boundaries or pinholes were synthesized as model nanostructures for the resistive switching bits. Consequently, the equivalent circuit models and electrochemistry can be treated purely by single crystalline oxide and contributions of the electrode|switching oxide interface.
- (iii) Good adhesion and contacting of both electrodes to the SrTiO<sub>3-δ</sub> thin film are simplifying the electrochemical setting. In contrast, studies, e.g., using AFM-based techniques suffer from tip–surface interaction, ill-defined electrical field, and geometry of the sampling area.

**A Bipolar Resistive Switching Process at Low Voltages.** The resistive switching response is strongly depending on the modification of the anionic-electronic carrier concentrations and fluxes with respect to the electric field

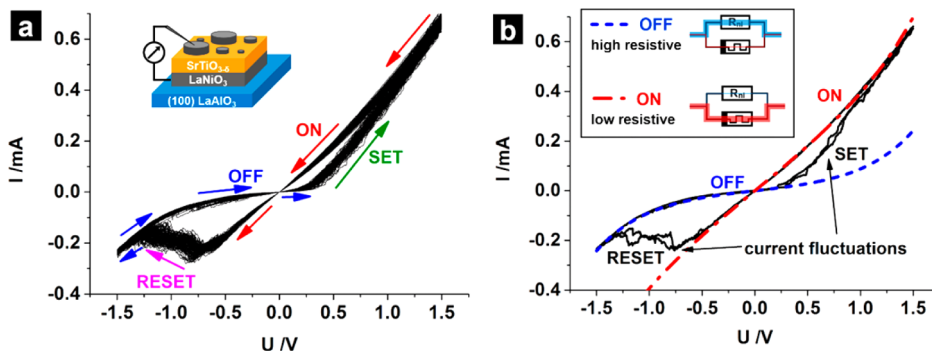


**Figure 2.** (a) Exemplary  $I$ – $V$  curves recorded for  $\pm 1.5$  V at 100 mV/s sweep rate. 100 consecutive cycles are shown proving stable bipolar resistive switching. ON/OFF as well as SET/RESET regimes during voltage cycling are indicated by arrows. (b) Two exemplary  $I$ – $V$  curves display the stochastic current variability during SET/RESET, and smooth ON/OFF states for which nonlinear least-squares fits are shown.

strengths applied. Therefore, we first characterize the model device structures in their hysteretic current–voltage ( $I$ – $V$ ) profiles by cyclic voltammetry. The circular memristive structures with top electrodes selectable between 40 and 320  $\mu\text{m}$  diameter reveal bipolar resistive switching, thus showing a pinched hysteretic  $I$ – $V$  curve with one crossover in the origin. This is exemplified in Figure 2, displaying the hysteretic  $I$ – $V$  profiles of a bit for  $\pm 1.5$  V sweep bias contacted over a 320  $\mu\text{m}$  diameter top-electrode area. The switching yielded highly repeatable  $I$ – $V$  profiles, and the reproducibility is demonstrated by the 100 consecutive cycles for 100 mV/s sweep rate displayed in Figure 2a. We observe switching, in counterclockwise direction of the positive  $I$ – $V$  branch for the voltage being applied to the top electrode. This means the device switches from a high resistance “OFF” state to a low resistance “ON” state at positive voltages and vice versa at negative voltages. Consequently, a SET region (OFF → ON) in the positive branch and a RESET region (ON → OFF) in the negative branch can be defined for the switch. All measured  $I$ – $V$  curves were highly reproducible already from the first cycles and did not require a forming step, which is sometimes reported in literature.<sup>2,9,40–42</sup> The reason for that might be the low SrTiO<sub>3- $\delta$</sub>  thickness of only 5 nm being ultrathin for a switch and the thereby resulting very high electric fields even at moderate voltages. In literature, a forming step is often argued with the formation of extended defects or conductive filaments. The measured data indicate that for the very thin films in this study, these processes are either fast or irrelevant, so that repeatable characteristics are already observed in the first  $I$ – $V$  cycles.

We now analyze the SET and RESET transitions in Figure 2b in more detail. In contrast to the smooth current changes with voltage in the ON or OFF state, we observe current fluctuations with sharp jumps in the SET/RESET range marked in Figure 2b. Such current fluctuations are attributed to nanoscale conductive filaments in oxygen anionic resistive switches.<sup>43–45</sup>

Assuming a locally highly confined region carrying most of the current under a high electric field, then even very small changes, *i.e.*, of individual atoms will cause a sudden change of the current flowing through the whole device. This results in stochastic current fluctuations during SET/RESET region as observable in Figure 2, see *e.g.* ref 44 for details.

Another indication for a filament-type switching mechanism besides the SET/RESET transitions can be found in the  $I$ – $V$  characteristics of the ON and OFF state. From Figure 2b, it is clear that while the ON state is almost ohmic, the OFF state has a strongly nonlinear  $I$ – $V$  relation. The almost ohmic  $I$ – $V$  characteristic with low resistance of the ON state suggests that ohmic resistivity of the tiny filament dominates the resistive contribution. To characterize the nonlinear  $I$ – $V$  relation of the OFF state, we use a double-exponential and symmetric fitting curve as often encountered in electrochemistry, which represents the OFF-state characteristics very well, see Figure 2b. Several effects can cause such an  $I$ – $V$  relation; in general, all processes are conceivable where the applied voltage influences an activation energy barrier for charge transfer. Here, in accordance with several reports in literature,<sup>40,46</sup> an electronic charge-transfer process at the SrTiO<sub>3- $\delta$</sub> |Pt interface can be expected as reason for the nonlinear  $I$ – $V$  characteristics.

Thorough analysis shows that two parallel conduction paths can represent the  $I$ – $V$  relations of the ON and OFF state: one nonlinear current path, which dominates the OFF state's  $I$ – $V$  characteristic and one ohmic path with a variable resistance depending on switching, which is the dominating current path in the ON state. We use a fitting model for the description of the ON state with an ohmic resistor and a parallel nonlinear path with the exact characteristics as observed in the OFF state showing excellent agreement with the slight nonlinearity of the ON state with voltage, see Figure 2b. The excellent fit of the ON state achieved by this model is a further indication for forming locally confined conductive filaments in the

ON state, as the OFF conduction path seems not altered, but only short-circuited.

In conclusion, we find for the ultrathin and epitaxial  $\text{SrTiO}_{3-\delta}$ -based bit structures a nonvolatile counterclockwise resistive switching process for operation with  $\pm 1.5$  V at 100 mV/s with statistic current fluctuations for the SET and RESET transitions. Hence, the ON state shows filamentary-type conduction, which is in agreement with reports in literature for  $\text{SrTiO}_{3-\delta}$  thin films and single crystals.<sup>13,15,20</sup> We now turn to investigate how larger modulations in field strength and sweep rate affect the resistive switching characteristics.

**Two Time- and Voltage-Dependent Competing Switching Processes.** A study on the effect of different voltages and sweep rates on the  $I$ - $V$  profiles measured on a single 320  $\mu\text{m}$  electrode is shown in Figure 3. We find that for the same sweep voltage but different sweep rate, the maximum positive and negative current, called  $I_{\text{SET}}/I_{\text{RESET}}$ ,<sup>12</sup> remain almost unchanged. Over the voltage-sweep rate variations, three different regimes are observed, exemplified by dashed lines in Figure 3. These regimes are the consequence of two different switching processes as explained in the following:

In regime I, at low voltages, the same filament-based counterclockwise process as introduced in the earlier section is observed. Here, we switch for the so-called first switching process in counterclockwise direction of the positive branch, Figure 3.

For regime II, at higher voltages, a second and additional hysteretic switching process occurs which is first observable at  $\pm 2.5$  V and for slow sweep rate (20 mV/s). This second process reveals also a stable bipolar switching mechanism, but of clockwise switching direction (in the positive branch). This process has therefore the opposite polarity compared to the first process observed at lower voltages. Analysis of the rather small opening of the  $I$ - $V$  hysteresis for fast sweep rates indicates rather slow kinetics for the second switch process. In regime II, both resistive switching processes are present with similar potency to form an  $I$ - $V$  hysteresis. Therefore, reproducible 2- or 3-crossover  $I$ - $V$  curves result as characteristics with respect to sweep rate and voltage.

Regime III, at the highest sweep voltage ( $\pm 4$  V) and lowest sweep rate (20 mV/s) shows a 1-crossover hysteretic and clockwise resistive switching process. Analysis of the  $I$ - $V$  profile reveals that the switching is in line with the second switching type observable already in regime II. In contrast to the first switching process, we observe no current fluctuations for the second switching process. This holds for its occurrence in both regimes II and III.

We demonstrate that ultrathin and epitaxial  $\text{SrTiO}_{3-\delta}$ -based bit structures can be operated to show either single crossover counterclockwise (regime I) or clockwise (regime III) switching or multicrossing  $I$ - $V$

profiles (regime II) depending on the sweep rate and electric field strength selected. This directly affects the respective SET and RESET currents as well as the memories' resistance states and switching directions. The SET/RESET processes described are highly reproducible, which is exemplified by the 100 cycles shown for each voltage and sweep rate combination exemplified in Figure 3. We observe two switching mechanisms, whereby the first switches from OFF to ON in the positive branch and reveals a filament-like origin for the low resistance ON state based on the fit analysis (Figure 2). In contrast, the second process switches from ON to OFF state in the positive branch and is investigated in further detail in this work. Literature comparison to single crystals and polycrystalline films of  $\text{SrTiO}_{3-\delta}$  reveals that the first switching process is comparable to defect-filament-based switching reported therein.<sup>13,15,20</sup> Earlier investigations on switching devices using  $\text{Sr}_2\text{TiO}_{4-\delta}$ ,<sup>41</sup> and Fe-doped  $\text{SrTiO}_{3-\delta}$ ,<sup>42</sup> reported the existence of both a clock- and counterclockwise switching process in the same resistive switching bit. Through this work, we conclude the following new insights: First, from a material perspective the occurrence of the two competing switching processes is independent of the iron doping and phase-polymorph change from  $\text{SrTiO}_{3-\delta}$  to  $\text{Sr}_2\text{TiO}_{4-\delta}$ . We report that in undoped and ultrathin  $\text{SrTiO}_{3-\delta}$  we can—in contrast to previous reports<sup>41,42</sup>—reproducibly address both processes in one and the same current voltage sweep and observe a superposition of the two competing switching mechanisms. The two processes are not only electric field strength dependent (e.g., as reported in ref 42) but importantly also charge flux and time dependent, Figure 3. This is in line with the basic formulation of the property of memristance,<sup>7,47</sup> and the systematic correlation of electric field strength-sweep rate dependence of the two switching processes is of use to define best operation schemes of the resistive switching bits. Third, our experiment on epitaxially grown bits reveals clearly that grain boundaries of the oxide material are not necessary sinks of defects responsible for the existence of the two competing resistive switching processes.

Based on the occurrence of those two mechanisms in undoped  $\text{SrTiO}_{3-\delta}$  bits and their implicated changes in switch direction and polarity, Figure 3, we further study the impact on the resistances values  $R_{\text{ON}}$  and  $R_{\text{OFF}}$  measured at low field strengths in Figure 4. For the analysis, we calculated a linear fit to the respective  $I$ - $V$  curve (Figure 3) for the region of  $\pm 100$  mV and extracted the resistance values from the slopes. As a general trend, upon increasing the sweep voltage an increase of  $R_{\text{OFF}}$  and a decrease of  $R_{\text{ON}}$  are observable for the first switching process (regime I). Upon further increase of the sweep voltage, this tendency is reversed by the presence of the second switching process (regime II). Thus, the  $R_{\text{OFF}}/R_{\text{ON}}$  ratio first

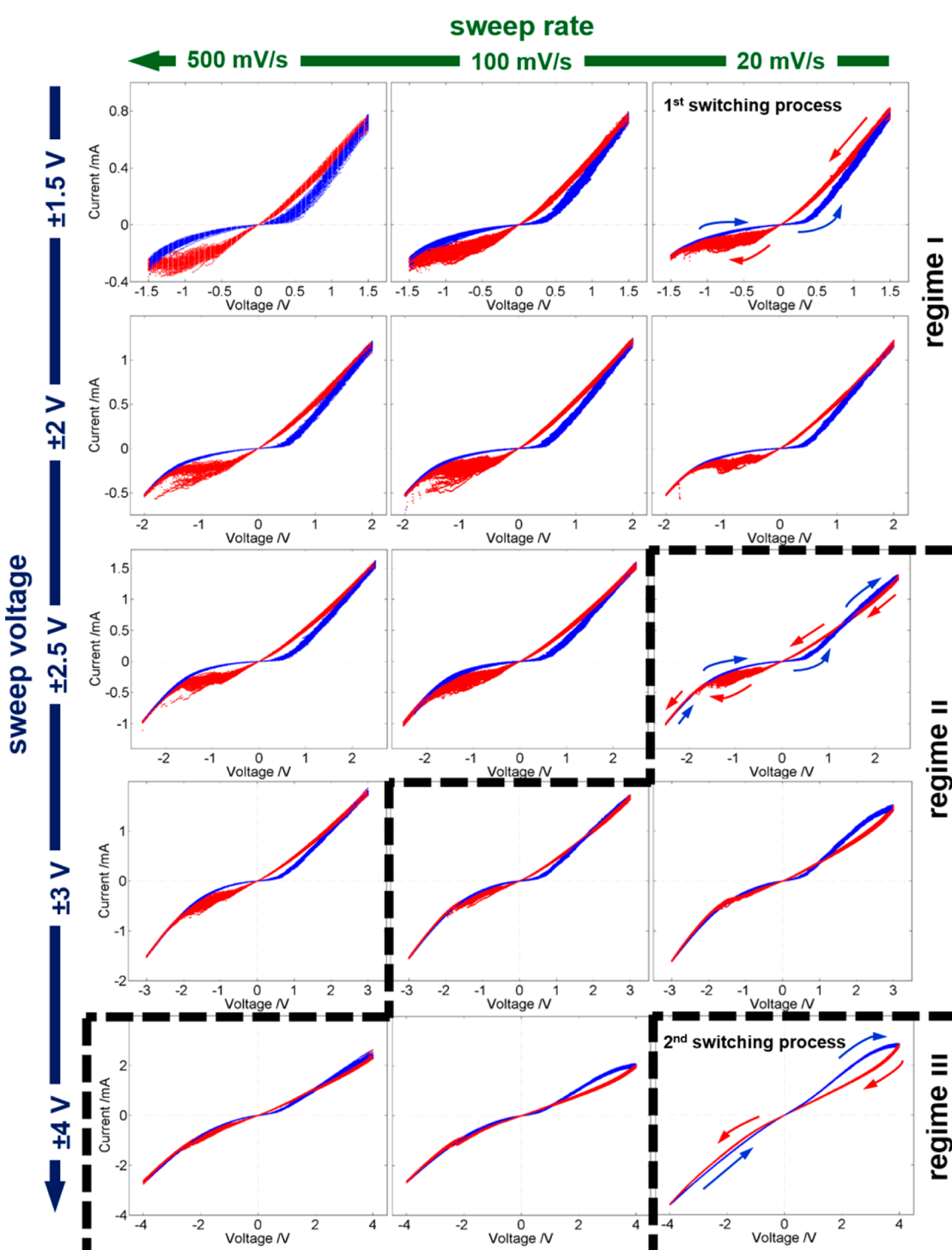


**Figure 3.** Cyclic voltammetry  $I$ – $V$  curves for different sweep rates (20 to 500 mV/s, right to left) and sweep voltages ( $\pm 1.5$  to  $\pm 4$  V, top to bottom). 100 consecutive cycles are shown for all conditions proving the stability of the switching processes. The blue curve represents increasing voltages, and the red curve decreasing voltages. Two independent bipolar switching processes with different polarity lead to three switching regimes: (I) counterclockwise 1-crossover hystereses; (II) a mixed regime with complicated 2–3 crossover curves; (III) clockwise 1-crossover hystereses.

increases to a value of about 10 at  $\pm 2$  V and then decreases again at higher sweep voltages. Lowering the sweep rate to 20 mV/s at highest applied voltage  $\pm 4$  V results in a change in bipolar switching polarity; whereby  $R_{ON}$  is now reached after negative voltages and  $R_{OFF}$  after positive voltages (regime III).

We now turn to further elucidate the characteristics of the first and second switching mechanisms by applying electrochemical AC methods. By using electrochemical impedance spectroscopy (EIS) it was possible to investigate the individual resistive and capacitive contributions of the device using equivalent

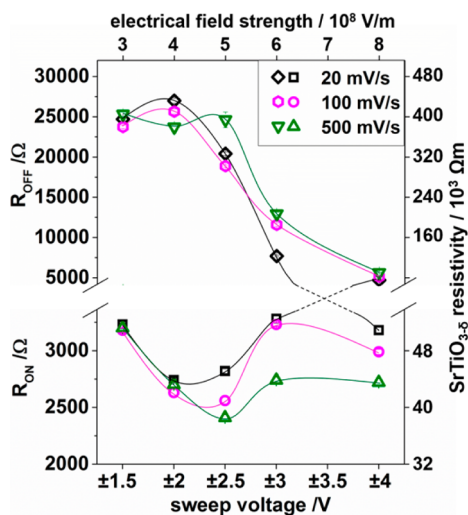


**Figure 4.** Evaluation of the ON and OFF resistances of the  $I$ - $V$  profiles shown in Figure 3. Error bars of the values from 100 cycles are shown, but are typically smaller than the symbols. The guidance lines follow the voltage polarity before reaching  $R_{ON}$ ,  $R_{OFF}$  and cross for  $\pm 4$  V 20 mV/s.

circuit models and connecting those to further mechanistic details.

**Separating Resistive and Capacitive Impedance Contributions of the ON and OFF States.** Electrical impedance spectroscopy using 10 mV<sub>AC</sub> amplitude was used to study the ON and OFF states according to the schematic in Figure 5a. As exemplified there, we now use short step functions or pulses of a certain voltage bias in the order of milliseconds and employ impedance spectroscopy to readout the resistive states. This differs from classic cyclic voltammetry for which the resistive switching and the readout of  $R_{ON}$  and  $R_{OFF}$  are always convoluted in a single voltage sweep. In the Nyquist plot displayed in Figure 5b, two typical impedance spectra of the ON and OFF state are shown for the first switching mechanism in counterclockwise direction and of bipolar and filamentary nature (regime I in Figure 3). Two features are clearly visible: First, a resistance  $R_1$ , visible as a high-frequency axis intercept. Second, an almost ideal semicircle composed of a resistance  $R_2$  with a capacitance  $C$  in parallel is determined. The equivalent circuit used for nonlinear-least-squares fit analysis consists of two resistances and a constant phase element (CPE) for considering non-idealities of the  $RC$  semicircle as shown in Figure 5b. Both the ON and OFF semicircles were almost ideal with a CPE exponent  $n = 0.96 \pm 0.01$  (note that for  $n = 1$  the CPE is equivalent to an ideal capacitance).<sup>48</sup> The capacitance  $C$  was determined from  $Q$  and  $n$ , the two fitting parameters of a constant phase element and the parallel resistance  $R_2$ , according to eq 1.<sup>49</sup> For both resistive states the same capacitance of  $\sim 3.7$  nF was extracted.

$$C = (R_2^{1-n} Q)^{1/n} \quad (1)$$

We study the resistance  $R_1$  and conclude, based on conductivity calculations and comparison to literature,<sup>50</sup>

that besides minor contributions from cables and tips, it is dominated by the LNO bottom electrode spreading resistance with a typical value of 700–800  $\Omega$  when using 320  $\mu\text{m}$  circular electrodes. In contrast, we find that the resistance  $R_2$  clearly changes with switching state and can be attributed to  $\text{SrTiO}_{3-\delta}$  with typical values of  $\sim 2$  and  $\sim 20$  k $\Omega$  for switching at 1.5 V from the low (ON) to the high (OFF) resistance state, see Figure 5b.

Figure 5c–e shows the results of such pulsed switching experiments with 10 ms switching for voltages  $\pm 1$  V and  $\pm 3$  V. Due to the relatively short switching pulses in this experiment, we observe predominantly the counterclockwise and first switching process, thus switching to ON with positive voltages, compare Figure 3, regime I. Importantly, we observe that the capacitance  $C$  as well as the electrode resistance  $R_1$  remain unchanged for all tested switching voltages or times, even though the resistance  $R_2$  changes significantly, see Figure 5d,e. Additional experiments with changed electrode size of the switches revealed that the capacitance scales as expected directly with electrode area and scales in the range of 4–5  $\mu\text{F}/\text{cm}^2$  for systematically changed electrode diameters (40–320  $\mu\text{m}$ ). Basic calculation of the films geometrical capacitance yields a roughly 1 order of magnitude higher capacitance of  $\sim 54$   $\mu\text{F}/\text{cm}^2$  (assuming a relative permittivity of the  $\text{SrTiO}_{3-\delta}$  film at room-temperature of  $\epsilon_r \sim 300$ ).<sup>51</sup> We tested the impact of increasing the oxide thickness by measuring an equivalent device with 50 nm  $\text{SrTiO}_{3-\delta}$  layer thickness. Interestingly, here we again find a capacitance in the order of  $\sim 5$   $\mu\text{F}/\text{cm}^2$  for the 50 nm  $\text{SrTiO}_{3-\delta}$  devices. Based on this we conclude that most probable effects of strain or high polarization are responsible for the unexpectedly low capacitances measured in 5 nm devices, as they are also shown in literature to strongly affect the relative permittivity.<sup>51–54</sup> While for 50 nm devices the capacitance and permittivity are already close to the expected values for bulk  $\text{SrTiO}_3$ . Also agglomerated defects as described in literature<sup>55,56</sup> could be responsible for lower permittivity at an interface, thus decreasing the total capacitive response by a small capacitance in series. We can, however, exclude polarization effects from the  $\text{LaNiO}_3$  bottom electrode which could reduce the active electrode area and thus the capacitance, by measuring the same  $R_1$  for ON and OFF state and by the direct dependency of capacitance to area for all electrode sizes.

Through impedance spectroscopy, we first access the characteristics of the ON and OFF states by addressing the first switching mechanisms which is filament-based. The  $R_{OFF}/R_{ON}$  ratio increased from 6 for  $\pm 1$  V to 25 for  $\pm 3$  V. We successfully demonstrate based on an impedance analysis approach that (i) the influence of the clockwise switching process is smaller at short switching times and (ii) that the electrode resistance ( $R_1$ ) can be separated in these AC read outs and

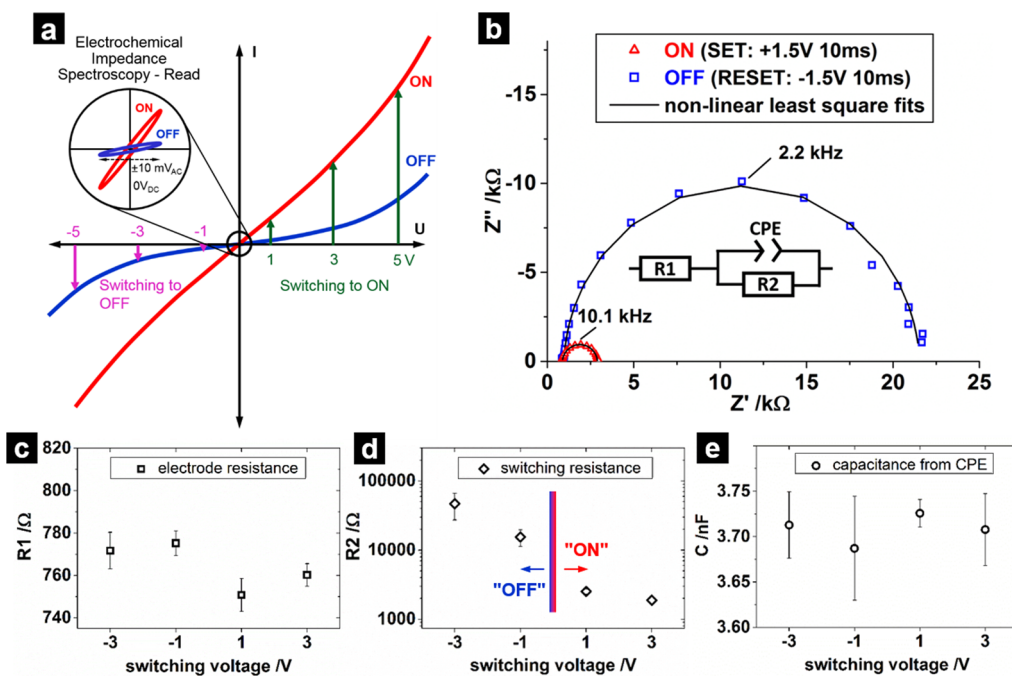


**Figure 5. Impedance spectroscopy of the ON and OFF state.** (a) Schematic of pulsed switching and subsequent testing of the resistive state by EIS. (b) Representative impedance spectra in Nyquist plot of the ON and OFF state and equivalent circuit model used for nonlinear least-squares fitting. (c–e) Resistance and capacitance values of 100 consecutive ON–OFF cycles at different switching voltages and 10 ms switching pulses. Using the equivalent circuit (b) for nonlinear-least-squares fitting of the spectra, the resistances  $R_1$  (c),  $R_2$  (d) and the capacitance  $C$  (e) are shown.

neglected as it does not contribute to the effective switching of the oxide resistance ( $R_2$ ).

It has to be noted that by using classic cyclic voltammetry ( $I$ – $V$  curves), these individual resistances and capacitances would not be extractable. Hence, EIS substantially improves the connection between the equivalent circuit models and switching mechanisms.

**Off-Equilibrium Electrochemical Impedance Analysis.** We now turn to study the characteristics of the second, clockwise switching process. For this, we perform impedance analysis at the switching conditions by potentiodynamic EIS, thus measuring AC impedance with DC biases applied to the resistive switch.

For these measurements, a large DC bias of  $\pm 1$ – $4$  V is first applied for 100 s to bring the sample to a stable nonequilibrium state. Then, on top of the same DC bias, a small 10 mV<sub>AC</sub> signal is applied to perform the impedance measurements, as exemplified in the schematic of Figure 6a. Thus, recorded impedance spectra are shown for the bits in Figure 6b,c. Samples were switched to the ON state of the counterclockwise first switching process before application of the DC biases by +1.5 V pulses, and resistive and capacitive contributions are discussed based on the equivalent circuit model using  $R_1$ ,  $R_2$ , and  $C$ .

In these measurements, the resistance  $R_1$  is almost constant at  $\sim 700$  Ω, which indicates that the LaNiO<sub>3</sub> electrodes remain unchanged even at high biases applied. For increasing positive biases, see Figure 6b,  $R_2$  first decreases with bias up to +2 V and then

increases again up to +4 V. At the same time, the almost ideal semicircle at low DC biases is strongly depressed at higher voltages. For negative DC bias, Figure 6c, the resistance  $R_2$  decreases for all voltages, and the semicircles retain their almost ideal shape. Comparing these results to observations made in the  $I$ – $V$  curves, we find for low bias, 0 to  $\pm 2$  V, the slightly nonlinear  $I$ – $V$  curves correspond in this experiment to a  $R_2$  resistance that is slowly decreasing with bias for both polarities. For  $\pm 3$  and  $\pm 4$  V, the clockwise switching process becomes apparent, increasing the resistance for positive bias and reducing the resistance even further at negative voltages.

Analyzing the capacitive responses, we note for voltages larger than  $\pm 1$  V bias a decrease, which is more pronounced at positive bias. Also for positive bias, an increased nonideality is observable, leading to strongly compressed RC semicircles for +3 and +4 V bias.

The reduced capacitances at large bias require attention. For thin-film SrTiO<sub>3</sub> is known that the permittivities of materials are reduced under high electric fields: Reductions of  $\epsilon_r$  by a factor of 3–10 are reported from zero electric field to  $10^7$  V/m.<sup>51,52</sup> Typically a symmetric decrease with electric field, independent of the polarization, can be expected. The differences in capacitance of a factor of 2.6 in our measurements with different bias  $\pm 4$  V clearly show a break in symmetry. We attribute this change in capacitance not only to a (field-symmetric) polarization of SrTiO<sub>3</sub> but also to a rearrangement of point- or extended defects under the

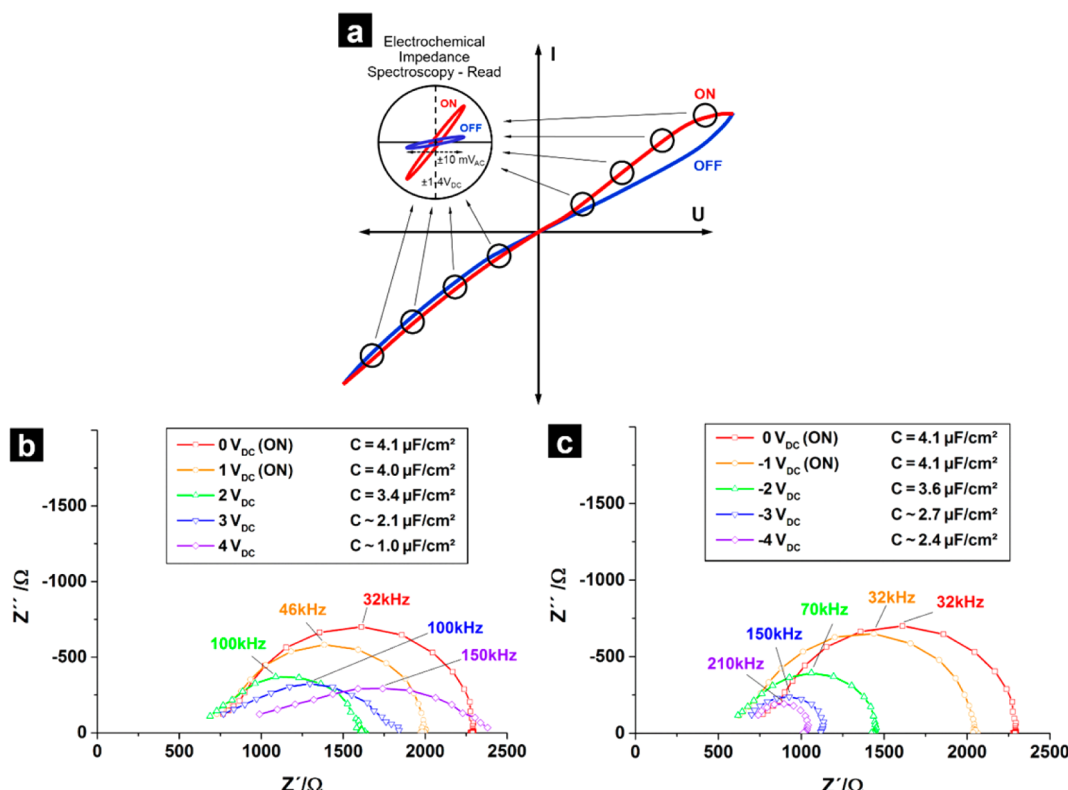


**Figure 6.** (a) Schematic of potentiodynamic impedance spectroscopy recorded with 10 mV<sub>AC</sub> after 100 s equilibration at applied DC voltages up to  $\pm 4$  V. The complex resistive and capacitive changes of the clockwise resistive switching process are shown under (b) positive and (c) negative bias load.

high fields causing asymmetric changes. Those asymmetric changes of capacitance/permittivity are with high probability directly associated with the also asymmetric bipolar switching behavior of the second process. At positive applied bias, oxygen vacancies would be driven toward the bottom electrode reducing their concentration as well as the concentration of charge balancing electrons close to the SrTiO<sub>3- $\delta$</sub> |Pt Schottky barrier. From the increase of resistance, we can conclude that this impedes the current flow through the device even if one or more conducting filaments are available (*i.e.*, the device is in ON state for the first process). We can further conclude from the nonideal, flat semicircles measured for high positive bias that no longer one uniform conduction process with a sharp frequency dispersion is present, but rather large differences in frequency for the resistive processes must exist. This is a strong indication toward an inhomogeneous resistance profile over the device. We interpret this either as local changes in charge carrier density in the oxide, or as thickness variation of a carrier-depleted zone near the top electrode. Similar thickness variations were reported in field-induced electro-coloration experiments of Fe-doped SrTiO<sub>3</sub> crystals.<sup>2</sup>

**Mechanistic Discussion.** We can summarize that at low voltages, a resistive switching process was characterized based on reversible formation of a conducting filament at positive voltage applied to the top

electrode and dissolution at negative voltages. This first process is responsible for bipolar counterclockwise resistive switching. The R<sub>OFF</sub>/R<sub>ON</sub> ratio of this process can be tuned by the switching voltage in the range of 5–25. The nonlinear I–V characteristics of the OFF state can be attributed to the Schottky barrier. In the ON state, the OFF-current path is still open, but it is in large amount short circuited by a laterally very confined low resistive conductive filament with ohmic I–V characteristics. The same capacitance is measured for both resistive states.

A second clockwise bipolar switching process (current decreasing at positive voltage and vice versa) with considerably slower switching kinetics is observed at high voltages. This process is independent from the first switching process, and combinations of the hysteretic I–V characteristics of the two processes are reproducibly observed at voltages  $\pm 2.5$  to  $\pm 4$  V leading to stable 2–3 crossover I–V characteristics. For  $\pm 4$  V and slow sweep rates this process becomes dominant, resulting in bipolar and clockwise single crossover curves. The capacitive contributions indicate that the high field strengths cause a significant redistribution of ionic and electronic charge carriers in the SrTiO<sub>3- $\delta$</sub>  thin film. In literature, oxygen vacancies and clusters of oxygen and strontium vacancies are suggested as redistributing ionic species in resistive switches of similar composition.<sup>42,55,56</sup> By the charge

carrier redistribution in our films, both the OFF and ON pathways of the first switching process are affected, and a superposition of both competing switching processes is observable for a certain switching voltage/time regime. As both processes are reversible and highly reproducible, this offers the possibility to tune the ON and OFF resistances and ratios and the overall electrochemical characteristics in an extremely broad range for a device, depending on the voltage and duration of the switching process.

## CONCLUSION

Resistive switches based on ultrathin 5 nm  $\text{SrTiO}_{3-\delta}$  thin films were successfully fabricated and tested. The PLD growth parameters have been optimized to achieve epitaxial and grain boundary-free growth of both the  $\text{LaNiO}_3$  bottom electrode and the switching material  $\text{SrTiO}_{3-\delta}$  itself as verified by XRD, TEM, and AFM. We clearly show that in this model system, two very different switching processes can be addressed in only 5 nm thick  $\text{SrTiO}_{3-\delta}$ -based switches. These two competing switching processes were characterized in detail: The first process induces counterclockwise (in the positive branch) bipolar resistive switching and is already active at low voltages of  $\pm 1.5$  V. The novel second process is responsible for clockwise bipolar resistive switching and is active at higher voltages starting from  $\pm 2.5$  V with slower kinetics than the first process.

From electrochemical measurements of ON/OFF states, the SET/RESET characteristics, changes of the

dielectric parameters with frequency as well as the bias dependent changes of the complex impedance, the following mechanistic features of the processes could be deduced: The first process is filament-based, and the nonlinear  $I-V$  characteristics of the OFF state are short-circuited by an ohmic current pathway in the ON state. The  $R_{\text{OFF}}/R_{\text{ON}}$  ratio of this process can be increased by a higher switching voltage thus affecting the conductive filament. At high voltages, however, a second bipolar switching process additionally influences the electric device characteristics. This second process coexists with the first switching process and affects the charge carriers at the  $\text{SrTiO}_{3-\delta}|\text{Pt}$  Schottky barrier. As both processes have different current–voltage–time characteristics, the two processes lead to a mixed regime with stable 2–3 crossover  $I-V$  profiles. At higher voltages and slower sweep rates, the clockwise process dominates the hysteretic response, leading to single 1-crossover clockwise resistive switching  $I-V$  curves.

By understanding the switching mechanistics and their connection to defect mechanisms and according models for  $\text{SrTiO}_{3-\delta}$  resistive switching, it is possible to extend the operation of the two different switching processes through a careful tuning of the effective voltage and time scales. Thereby the  $R_{\text{OFF}}/R_{\text{ON}}$  ratio and single to multiple crossovers of the resistive switches cyclic voltammetry response can be addressed offering new performance implication metrics for memristor-based circuits and novel device functionality.

## MATERIALS AND METHODS

**Resistive Switching Materials and Device Fabrication.** Bilayers of  $\text{LaNiO}_3$  (bottom electrode) and  $\text{SrTiO}_{3-\delta}$  (switching oxide) were grown on top of epi-polished single crystalline (100)  $\text{LaAlO}_3$  substrates (CrysTec, Germany) by pulsed laser deposition (PLD) using a KrF (248 nm) excimer laser (COMPEx Pro 220 F). The following growth parameters were optimized individually to achieve epitaxial layer-by-layer growth for both  $\text{LaNiO}_3$  and  $\text{SrTiO}_{3-\delta}$  films, respectively: laser energy ( $0.9 \text{ J/cm}^2$ ,  $1.0 \text{ J/cm}^2$ ), pulse frequency (2 Hz, 2 Hz), background  $\text{O}_2$  pressure (0.03 mbar, 0.02 mbar), and temperature ( $500^\circ\text{C}$ ,  $650^\circ\text{C}$ ). Film thicknesses of 10 nm ( $\text{LaNiO}_3$ ) and 5 nm ( $\text{SrTiO}_{3-\delta}$ ) were controlled via the deposition time.

For  $\text{LaNiO}_3$  depositions, the PLD target was prepared via a nitrate-citrate (Pechini-type) synthesis using  $\text{La}(\text{NO}_3)_3 \cdot 6\text{H}_2\text{O}$  (99.9%, Alfa Aesar),  $\text{Ni}(\text{NO}_3)_2 \cdot 6\text{H}_2\text{O}$  (99.9%, Strem chemicals), citric acid (99%, Aldrich), ethylene glycol (99.5%, Fluka), and nitric acid (puriss p.a., Sigma-Aldrich). The resulting powder was hot-pressed at  $700^\circ\text{C}$  and 2 MPa and then annealed at  $800^\circ\text{C}$  in air to remove carbon. Phase purity of the target was confirmed by XRD. A single crystalline commercial target (Crystec, Germany) was used for  $\text{SrTiO}_{3-\delta}$  deposition.

The 80 nm thick Pt top electrodes were deposited by e-beam evaporation (Plasys MEB 550, France) through a shadow mask, after removing organic traces by  $\text{O}_2$  plasma ashing. Thereby, a total number of 80 circular model electrodes of diameters 40, 80, 160, and  $320 \mu\text{m}$  were prepared for electrical and electrochemical measurements.

**Structure, Chemistry, and Nanostructure Characterization.** XRD was performed on the  $\text{LaNiO}_3$  PLD-target (Bruker D8) and on bilayer films of  $\text{LaNiO}_3$  and  $\text{SrTiO}_{3-\delta}$  grown on (100)  $\text{LaAlO}_3$  (Seifert

3003 PTS-HR) in Bragg–Brentano geometry using  $\text{Cu K}\alpha$  wavelength.

HR-TEM and scanning transmission electron microscopy measurements were performed (FEI Tecnai F30) at 300 kV to investigate layer growth and possible nanoscale defects in the epitaxial oxide thin films. Samples for TEM were cut and thinned from a characterized resistive switching bit by focused ion beam (FIB) technique using a 30 kV, 300 pA gallium ion beam (NVision 40, Zeiss).

AFM (Cypher S, Asylum Research) was used to characterize the surface morphology of  $\text{LaNiO}_3|\text{SrTiO}_{3-\delta}$  bilayers grown on (100)  $\text{LaAlO}_3$  in AC tapping mode (Arrow NCR-tips, NanoWorld).

**Electrochemical Testing of Resistive Switching Characteristics.** We employ a rather unusually wide combination of electrochemical methods to investigate the resistive and capacitive contributions of high and low resistive states at low readout bias and also at the off-equilibrium conditions at which the switching processes occur. Such methods allow direct mechanistic insights on the operation principles and are not state-of-the-art to study electrochemical properties of memristors. For this study, electrochemical AC and DC measurements including cyclic voltammetry, chronoamperometry, EIS, and potentiodynamic EIS were performed with a potentiostat/galvanostat/impedance analyzer (Gamry Instruments, Reference 600) at room temperature in air using an electrically shielded setup. Microelectrodes were contacted via custom-made Pt tips using 3D micropositioners (Everbeing, Taiwan). Cyclic voltammetry measurements were done in the range from  $\pm 1.5$  to  $\pm 4$  V with sweep rates 20–500 mV/s as for voltages higher than  $\pm 5$  V, a degradation effect, namely irreversible increase of the ON state resistance is observed. EIS was performed in potentiostatic mode

with 10 mV<sub>AC</sub> (rms) amplitude. The frequency range from 100 mHz to 1 MHz was selected for investigation. For successful measurements, we adapted and reduced the frequency range to increase measurement speed, if no dielectric contributions were expected in the respective frequency range. Voltages displayed in figures and discussed in the text were always applied to the top (Pt) electrodes for all measurements in this study.

*Conflict of Interest:* The authors declare no competing financial interest.

*Acknowledgment.* The authors thank Dr. M. Trassin for his support with epitaxial film growth, Dr. A. Sologubenko from the Scientific Center for Optical and Electron Microscopy ScopeM of the Swiss Federal Institute of Technology ETHZ for TEM-imaging and Prof. P. Gambardella for AFM access. Financial support by Swiss National Science Foundation projects 138914 and 144988 is gratefully acknowledged.

## REFERENCES AND NOTES

- Waser, R.; Aono, M. Nanoionics-Based Resistive Switching Memories. *Nat. Mater.* **2007**, *6*, 833–840.
- Waser, R.; Dittmann, R.; Staikov, G.; Szot, K. Redox-Based Resistive Switching Memories - Nanoionic Mechanisms, Prospects, and Challenges. *Adv. Mater.* **2009**, *21*, 2632.
- Strukov, D. B.; Snider, G. S.; Stewart, D. R.; Williams, R. S. The Missing Memristor Found. *Nature* **2008**, *453*, 80–83.
- Wong, H. S. P.; Heng-Yuan, L.; Shimeng, Y.; Yu-Sheng, C.; Yi, W.; Pang-Shiu, C.; Byoungil, L.; Chen, F. T.; Ming-Jinn, T. Metal Oxide RRAM. *Proc. IEEE* **2012**, *100*, 1951–1970.
- Hickmott, T. W. Low-Frequency Negative Resistance in Thin Anodic Oxide Films. *J. Appl. Phys.* **1962**, *33*, 2669–2682.
- Gibbons, J. F.; Beadle, W. E. Switching Properties of Thin Nio Films. *Solid-State Electron.* **1964**, *7*, 785–790.
- Chua, L. O. Memristor-the Missing Circuit Element. *IEEE Trans. Circuit Theory* **1971**, *18*, 507–519.
- International Technology Roadmap for Semiconductors, 2011 edition, <http://www.itrs.net/>.
- Guo, X. Roles of Schottky Barrier and Oxygen Vacancies in the Electroforming of SrTiO<sub>3</sub>. *Appl. Phys. Lett.* **2012**, *101*, 152903.
- Strukov, D. B.; Borghetti, J. L.; Williams, R. S. Coupled Ionic and Electronic Transport Model of Thin-Film Semiconductor Memristive Behavior. *Small* **2009**, *5*, 1058–1063.
- Sawa, A. Resistive Switching in Transition Metal Oxides. *Mater. Today* **2008**, *11*, 28–36.
- Messerschmitt, F.; Kubicek, M.; Schweiger, S.; Rupp, J. L. M. Memristor Kinetics and Diffusion Characteristics for Mixed Anionic-Electronic SrTiO<sub>3-Δ</sub> Bits: The Memristor-Based Cottrell Analysis Connecting Material to Device Performance. *Adv. Funct. Mater.* **2014**, *24*, 7448–7460.
- Muenstermann, R.; Dittmann, R.; Szot, K.; Mi, S.; Jia, C.-L.; Meuffels, P.; Waser, R. Realization of Regular Arrays of Nanoscale Resistive Switching Blocks in Thin Films of Nb-Doped SrTiO<sub>3</sub>. *Appl. Phys. Lett.* **2008**, *93*, 023110.
- Jia, C. L.; Houben, L.; Urban, K. Atom Vacancies at a Screw Dislocation Core in SrTiO<sub>3</sub>. *Philos. Mag. Lett.* **2006**, *86*, 683–690.
- Szot, K.; Speier, W.; Bihlmayer, G.; Waser, R. Switching the Electrical Resistance of Individual Dislocations in Single-Crystalline SrTiO<sub>3</sub>. *Nat. Mater.* **2006**, *5*, 312–320.
- Metlenko, V.; Ramadan, A. H. H.; Gunkel, F.; Du, H.; Schraknepper, H.; Hoffmann-Eifert, S.; Dittmann, R.; Waser, R.; De Souza, R. A. Do Dislocations Act as Atomic Autobahns for Oxygen in the Perovskite Oxide SrTiO<sub>3</sub>? *Nanoscale* **2014**, *6*, 12864–12876.
- Marrocchelli, D.; Sun, L.; Yildiz, B. Dislocations in SrTiO<sub>3</sub>: Easy to Reduce but Not So Fast for Oxygen Transport. *J. Am. Chem. Soc.* **2015**, *137*, 4735.
- Yang, J. J.; Pickett, M. D.; Li, X. M.; Ohlberg, D. A. A.; Stewart, D. R.; Williams, R. S. Memristive Switching Mechanism for Metal/Oxide/Metal Nanodevices. *Nat. Nanotechnol.* **2008**, *3*, 429–433.
- Ielmini, D. Modeling the Universal Set/Reset Characteristics of Bipolar RRAM by Field- and Temperature-Driven Filament Growth. *IEEE Trans. Electron Devices* **2011**, *58*, 4309–4317.
- Menke, T.; Meuffels, P.; Dittmann, R.; Szot, K.; Waser, R. Separation of Bulk and Interface Contributions to Electroforming and Resistive Switching Behavior of Epitaxial Fe-Doped SrTiO<sub>3</sub>. *J. Appl. Phys.* **2009**, *105*, 066104.
- Yu, S.; Guan, X.; Wong, H. S. P. Conduction Mechanism of Tin/HfO<sub>x</sub>/Pt Resistive Switching Memory: A Trap-Assisted-Tunneling Model. *Appl. Phys. Lett.* **2011**, *99*, 063507.
- Asanuma, S.; Akoh, H.; Yamada, H.; Sawa, A. Relationship between Resistive Switching Characteristics and Band Diagrams of Ti|Pr<sub>1-x</sub>CaxMnO<sub>3</sub> Junctions. *Phys. Rev. B: Condens. Matter Mater. Phys.* **2009**, *80*, 235113.
- Fujii, T.; Kawasaki, M.; Sawa, A.; Kawazoe, Y.; Akoh, H.; Tokura, Y. Electrical Properties and Colossal Electroresistance of Heteroepitaxial SrRuO<sub>3</sub>/SrTi<sub>1-x</sub>Nb<sub>x</sub>O<sub>3</sub> 0.0002<sub>x</sub>\0.02 Schottky Junctions. *Phys. Rev. B: Condens. Matter Mater. Phys.* **2007**, *75*, 165101.
- Russo, U.; Ielmini, D.; Cagli, C.; Lacaita, A. L.; Spiga, S.; Wiemer, C.; Perego, M.; Fanciulli, M. In Conductive-Filament Switching Analysis and Self-Accelerated Thermal Dissolution Model for Reset in NiO-Based RRAM. *IEEE International Electron Devices Meeting*, 2007 (IEDM 2007), Washington, DC, December 10–12, 2007; IEEE: New York, **2007**; pp 775–778.
- Messerschmitt, F.; Kubicek, M.; Rupp, J. L. M. How Does Moisture Affect the Physical Property of Memristance for Anionic-Electronic Resistive Switching Memories? *Adv. Funct. Mater.* **2015**, *25*, 5117–5125.
- Tappertzhofen, S.; Valov, I.; Tsuruoka, T.; Hasegawa, T.; Waser, R.; Aono, M. Generic Relevance of Counter Charges for Cation-Based Nanoscale Resistive Switching Memories. *ACS Nano* **2013**, *7*, 6396–6402.
- Park, J.; Lee, S.; Lee, J.; Yong, K. A Light Incident Angle Switchable Zno Nanorod Memristor: Reversible Switching Behavior between Two Non-Volatile Memory Devices. *Adv. Mater.* **2013**, *25*, 6423–6429.
- Yildiz, B. Stretching the Energy Landscape of Oxides—Effects on Electrocatalysis and Diffusion. *MRS Bull.* **2014**, *39*, 147–156.
- Schweiger, S.; Kubicek, M.; Messerschmitt, F.; Murer, C.; Rupp, J. L. M. A Microdot Multilayer Oxide Device: Let Us Tune the Strain-Ionic Transport Interaction. *ACS Nano* **2014**, *8*, 5032–5048.
- Ohring, M. Film Structure. In *Materials Science of Thin Films* (2nd ed.; Ohring, M., Ed. Academic Press: San Diego, CA, 2002; Chpt 9, pp 495–558.
- Merkle, R.; Maier, J. How Is Oxygen Incorporated into Oxides? A Comprehensive Kinetic Study of a Simple Solid-State Reaction with SrTiO<sub>3</sub> as a Model Material. *Angew. Chem., Int. Ed.* **2008**, *47*, 3874–3894.
- Rothschild, A.; Meneskou, W.; Tuller, H. L.; Ivers-Tiffée, E. Electronic Structure, Defect Chemistry, and Transport Properties of SrTi<sub>1-x</sub>Fe<sub>x</sub>O<sub>3-y</sub> Solid Solutions. *Chem. Mater.* **2006**, *18*, 3651–3659.
- De Souza, R. A.; Metlenko, V.; Park, D.; Weirich, T. E. Behavior of Oxygen Vacancies in Single-Crystal SrTiO<sub>3</sub>: Equilibrium Distribution and Diffusion Kinetics. *Phys. Rev. B: Condens. Matter Mater. Phys.* **2012**, *85*, 174109-1–174109-11.
- Nili, H.; et al. Donor-Induced Performance Tuning of Amorphous SrTiO<sub>3</sub> Memristive Nanodevices: Multistate Resistive Switching and Mechanical Tunability. *Adv. Funct. Mater.* **2015**, *25*, 3172–3182.
- Ohring, M. Substrate Surfaces and Thin-Film Nucleation. In *Materials Science of Thin Films*, 2nd ed.; Ohring, M., Ed.; Academic Press: San Diego, CA, 2002; Chpt. 7, pp 357–415.
- Lehnert, H.; Boysen, H.; Dreier, P.; Yu, Y. Room Temperature Structure of Al<sub>2</sub>O<sub>3</sub>. *Z. Kristallogr. - Cryst. Mater.* **2000**, *215*, 145–147.
- Blasco, J.; Sánchez, M. C.; Pérez-Cacho, J.; García, J.; Subías, G.; Campo, J. Synthesis and Structural Study of LaNi<sub>1-x</sub>Mn<sub>x</sub>O<sub>3+Δ</sub> Perovskites. *J. Phys. Chem. Solids* **2002**, *63*, 781–792.

38. Levin, A. A.; Paufler, P.; Meyer, D. C. Low-Temperature Domain Behaviour of a  $\text{SrTiO}_3$  (001) Single-Crystal Plate. *Phys. B* **2007**, *393*, 373–381.
39. Kiessig, H. Untersuchungen Zur Totalreflexion Von Röntgenstrahlen. *Ann. Phys.* **1931**, *402*, 715–768.
40. Dittmann, R.; et al. Scaling Potential of Local Redox Processes in Memristive  $\text{SrTiO}_3$  Thin-Film Devices. *Proc. IEEE* **2012**, *100*, 1979–1990.
41. Shibuya, K.; Dittmann, R.; Mi, S.; Waser, R. Impact of Defect Distribution on Resistive Switching Characteristics of  $\text{Sr}_2\text{TiO}_4$  Thin Films. *Adv. Mater.* **2010**, *22*, 411–414.
42. Muenstermann, R.; Menke, T.; Dittmann, R.; Waser, R. Coexistence of Filamentary and Homogeneous Resistive Switching in Fe-Doped  $\text{SrTiO}_3$  Thin-Film Memristive Devices. *Adv. Mater.* **2010**, *22*, 4819–4822.
43. Guan, X.; Shimeng, Y.; Wong, H. S. P. On the Switching Parameter Variation of Metal-Oxide RRAM; Part I: Physical Modeling and Simulation Methodology. *IEEE Trans. Electron Devices* **2012**, *59*, 1172–1182.
44. Ambrogio, S.; Balatti, S.; Cubeta, A.; Calderoni, A.; Ramaswamy, N.; Ielmini, D. Statistical Fluctuations in  $\text{HfO}_x$  Resistive-Switching Memory: Part I - Set/Reset Variability. *IEEE Trans. Electron Devices* **2014**, *61*, 2912–2919.
45. Chen, F. T., et al. In *Resistance Instabilities in a Filament-Based Resistive Memory*, IEEE International Reliability Physics Symposium (IRPS), 2013, Monterey, CA, April 14–18, 2013; IEEE: New York, **2013**, pp 5E.1.1–5E.1.7.
46. Yin, X.-B.; Tan, Z.-H.; Guo, X. The Role of Schottky Barrier in the Resistive Switching of  $\text{SrTiO}_3$ : Direct Experimental Evidence. *Phys. Chem. Chem. Phys.* **2015**, *17*, 134–137.
47. Yang, J. J.; Borghetti, J.; Murphy, D.; Stewart, D. R.; Williams, R. S. A Family of Electronically Reconfigurable Nanodevices. *Adv. Mater.* **2009**, *21*, 3754–3758.
48. Shoar Abouzari, M. R.; Berkeemeier, F.; Schmitz, G.; Wilmer, D. On the Physical Interpretation of Constant Phase Elements. *Solid State Ionics* **2009**, *180*, 922–927.
49. Fleig, J. The Grain Boundary Impedance of Random Microstructures: Numerical Simulations and Implications for the Analysis of Experimental Data. *Solid State Ionics* **2002**, *150*, 181–193.
50. Rajeev, K. P.; Shivashankar, G. V.; Raychaudhuri, A. K. Low-Temperature Electronic Properties of a Normal Conducting Perovskite Oxide ( $\text{LaNiO}_3$ ). *Solid State Commun.* **1991**, *79*, 591–595.
51. Hao, J. H.; Luo, Z.; Gao, J. Effects of Substrate on the Dielectric and Tunable Properties of Epitaxial  $\text{SrTiO}_3$  Thin Films. *J. Appl. Phys.* **2006**, *100*, 114107.
52. Antons, A.; Neaton, J. B.; Rabe, K. M.; Vanderbilt, D. Tunability of the Dielectric Response of Epitaxially Strained  $\text{SrTiO}_3$  from First Principles. *Phys. Rev. B: Condens. Matter Mater. Phys.* **2005**, *71*, 024102.
53. Hyun, S.; Char, K. Effects of Strain on the Dielectric Properties of Tunable Dielectric  $\text{SrTiO}_3$  Thin Films. *Appl. Phys. Lett.* **2001**, *79*, 254–256.
54. Kim, L.; Jung, D.; Kim, J.; Kim, Y. S.; Lee, J. Strain Manipulation in  $\text{BaTiO}_3/\text{SrTiO}_3$  Artificial Lattice toward High Dielectric Constant and Its Nonlinearity. *Appl. Phys. Lett.* **2003**, *82*, 2118–2120.
55. Su Kim, Y.; et al. Impact of Vacancy Clusters on Characteristic Resistance Change of Nonstoichiometric Strontium Titanate Nano-Film. *Appl. Phys. Lett.* **2014**, *104*, 013501.
56. Lee, S.; Lee, J. S.; Park, J.-B.; Koo Kyoung, Y.; Lee, M.-J.; Won Noh, T. Anomalous Effect Due to Oxygen Vacancy Accumulation Below the Electrode in Bipolar Resistance Switching Pt/Nb:SrTiO<sub>3</sub> Cells. *APL Mater.* **2014**, *2*, 066103.